



Article

Synthesis of CuO/ZnO Nanocomposites and Their Application in Photodegradation of Toxic Textile Dye

Abdullah Al Mamun Sakib ¹, Shah Md. Masum ¹, Jan Hoinkis ², Rafiqul Islam ¹ and Md. Ashraful Islam Molla ^{1,*}

¹ Department of Applied Chemistry & Chemical Engineering, Faculty of Engineering & Technology, University of Dhaka, Dhaka 1000, Bangladesh; abdullahsakib33@gmail.com (A.A.M.S.); masumdhk@yahoo.com (S.M.M.); professorrafiqulislam@yahoo.co.uk (R.I.)

² Centre of Applied Research (CAR), Karlsruhe University of Applied Sciences, 76133 Karlsruhe, Germany; jan.hoinkis@hs-karlsruhe.de

* Correspondence: ashraful.acce@du.ac.bd

Received: 23 August 2019; Accepted: 13 September 2019; Published: 17 September 2019



Abstract: CuO/ZnO composites are synthesized using a simple mechanochemical combustion method. X-ray diffraction (XRD), scanning electron microscopy (SEM), energy-dispersive X-ray spectroscopy (EDX), and Fourier transform infrared (FTIR) are used to characterize the prepared oxides. X-ray diffraction reveals that the prepared CuO/ZnO exhibit a wurtzite ZnO crystal structure and the composites are composed of CuO and ZnO. The strong peaks of the Cu, Zn, and O elements are exhibited in the EDX spectrum. The FTIR spectra appear at around 3385 cm⁻¹ and 1637 cm⁻¹, caused by O–H stretching, and 400 cm⁻¹ to 590 cm⁻¹, ascribable to Zn–O stretching. The photocatalytic performances of CuO/ZnO nanocomposites are investigated for the degradation of methylene blue (MB) aqueous solution in direct solar irradiation. The degradation value of MB with 5 wt % CuO/ZnO is measured to be 98%, after 2 h of solar irradiation. The reactive •O₂⁻ and •OH radicals play important roles in the photodegradation of MB. Mineralization of MB is around 91% under sunlight irradiation within 7 h. The photodegradation treatment for the textile wastewater using sunlight is an easy technique—simply handled, and economical. Therefore, the solar photodegradation technique may be a very effective method for the treatment of wastewater instead of photodegradation with the artificial and expensive Hg-Xe lamp.

Keywords: CuO/ZnO; photodegradation; nanocomposite; methylene blue; sunlight

1. Introduction

It is evident that water pollution is a global environmental problem now due to the presence of different types of hazardous pollutants in it [1]. Textile wastewater, which contains huge amounts of pollutants that are very harmful to the environment, is of special research interest. The release of textile wastewater to the environment causes aesthetic problems due to the changed color of the water bodies [2]. Nanocomposites, containing oxides of metal, are of great research interest at the moment due to their high photocatalytic degradation efficiency, sustainable development characteristics, and lack of secondary pollution for water pollution treatment [3,4]. Recently, different types of metal oxide nanocomposites have been synthesized, such as ZnO–Mg [5], CuO/ZnO [6], ZnO–NiO [7], Co₃O₄–ZnO [8], and CeO₂–ZnO [9]. Saravanan et al. prepared CuO/ZnO, V₂O₅/ZnO, and ZnO/γ-Mn₂O₃ nanocomposites using the thermal decomposition method [10–12]. They also studied the photocatalytic degradation of rhodamine B under sunlight irradiation using CuO/ZnO nanocomposite. Li et al. [13] synthesized CuO/ZnO nanocomposites using the thermal decomposition method and investigated the visible light-driven photocatalytic degradation of methylene blue and

methyl orange. Kuriakose et al. [14] prepared CuO/ZnO nanocomposites using the carbothermal evaporation method and evaluated the photocatalytic degradation of methylene blue and methyl orange dyes under sunlight irradiation. Wang et al. [15] prepared MnO@MnOx microspheres through the solvothermal process and reported the degradation of levofloxacin under simulated sunlight irradiation. Nanocomposite photocatalytic technology can be considered a green technology and provides the advantages of abundance, including postpone electron-hole recombination, higher photocatalytic activity, and the ability to convert solar energy to chemical energy, which eventually realizes the solution of energy and environmental issues [16–21].

ZnO is an n-type semiconductor, having a conductivity of about 10^{-7} – 10^{-3} S/cm. It has a relatively large binding energy of 60 meV. However, the main disadvantages of ZnO are its fast electron-hole recombination rate and inefficient utilization of sunlight that lead to a reduction in photodegradation efficiency. The photodegradation performance of ZnO can be increased by modifying ZnO with transition metals [22]. Among the various transition metals, Cu-doped ZnO nanomaterials are of special interest due to the photocatalytic efficiency enhancement that creates defects in the lattice and reduces the recombination of photogenerated charge carriers [23]. Cu also provides plenty of advantages, such as low cost, more electronegativity than zinc, and a similar atomic size to that of zinc, and leads to better doping efficiency [24]. CuO is a natural p-type semiconductor with a narrow band gap, having a conductivity of 10^{-4} S/cm, and it can be applied in photodegradation reactions [25]. Among the various metal oxide nanocomposites, researchers are paying more attention to CuO/ZnO because of its non-toxicity, economical benefits, and availability. It possesses high energy density and good electrical and piezoelectric properties [26,27]. CuO/ZnO nanocomposites improve physicochemical properties, compared to pure ZnO and CuO nanostructures [14]. The formation of a CuO/ZnO heterojunction also enhances the optical and electronic properties, which are considered to be promising applications in photocatalysis [10].

Herein, the various proportions of CuO/ZnO nanocomposites are prepared using the mechanochemical combustion method. The synthesized composites are characterized by X-ray diffraction (XRD), scanning electron microscopy (SEM), energy-dispersive X-ray spectroscopy (EDX), and Fourier transform infrared (FTIR). Methylene blue (MB) is a non-biodegradable and hazardous organic compound intensively used in textile industries and, so, it is selected as the degradation target to evaluate the photocatalytic performances of the composites using sunlight. The results show that CuO/ZnO exhibit increased photocatalytic activities, compared with ZnO. The degradation mechanism and mineralization of the improved photocatalytic performance are also discussed.

2. Materials and Methods

2.1. Chemicals

The samples were synthesized using zinc acetate dihydrate ($\text{Zn}(\text{CH}_3\text{COO})_2 \cdot 2\text{H}_2\text{O}$), oxalic acid dihydrate ($(\text{COOH})_2 \cdot 2\text{H}_2\text{O}$), and copper acetate ($\text{Cu}(\text{CH}_3\text{COO})_2$). Methylene blue ($\text{C}_{16}\text{H}_{18}\text{ClN}_3\text{S}$) was employed in the photodegradation experiment. Three scavengers were selected: Ascorbic acid ($\text{C}_6\text{H}_8\text{O}_6$), 2-propanol ($(\text{CH}_3)_2\text{CHOH}$), and di-ammonium oxalate monohydrate ($(\text{NH}_4)_2\text{C}_2\text{O}_4 \cdot \text{H}_2\text{O}$). All of the analytical grade chemicals were used without any purification.

2.2. Fabrication of CuO/ZnO

The mechanochemical combustion method was used to prepare CuO/ZnO. In agitate mortar, 2.195 g of zinc oxalate dihydrate and 2.521 g of acetic acid were taken. Then, the mixture was ground for 10 min to produce $\text{Zn}(\text{CH}_3\text{COO})_2 \cdot 2\text{H}_2\text{O}$ and $(\text{COOH})_2 \cdot 2\text{H}_2\text{O}$ paste. In the above paste, $\text{Cu}(\text{CH}_3\text{COO})_2$ was added as a source of Cu, and then the grinding process was continued for the next 10 min to produce a precursor of zinc oxalate–copper oxalate. The precursor powders were calcined at 500 °C for 3 h in the presence of air atmosphere to obtain the CuO/ZnO composite [28]. For comparison, un-doped ZnO was prepared from the zinc oxalate and acetic acid paste.

2.3. Characterization

The X-ray diffractometer (XRD, Ultima IV, Rigaku Corporation, Akishima, Japan) was selected to collect the diffraction patterns of materials using Cu K α radiation ($\lambda = 0.15406$ nm, 40 KV, 1.64 mA) in the ranges of 10° to 80° of 2-theta angle. The morphologies of oxides were recorded with a scanning electron microscope (SEM, JSM-6010 PLUS/LA, JEOL Ltd., Tokyo, Japan). Elemental analysis of CuO/ZnO was examined using a JSM-7900F SEM attached with EDX. The chemical structures of CuO/ZnO were studied with a Fourier transform infrared (FTIR) spectrophotometer (IR Prestige-21, SHIMADZU, Kyoto, Japan).

2.4. Evaluation of Photocatalytic Activity

The photocatalytic experimental conditions are presented in Table 1. Briefly, the photocatalytic performance of CuO/ZnO composites was investigated in aqueous MB solution using sunlight. Experiments were conducted under similar conditions on a sunny day between 11:00 and 14:00. In photodegradation, 20 mg of photocatalyst was added into 30 mL aqueous MB of 10 mg/L in the beakers. To equilibrate the suspension, a magnetic stirrer was used in the dark for 30 min. Then, the suspensions in the beakers were kept in sunlight for different time intervals. About 3 mL MB solution was withdrawn and separated with an Advantec membrane filter 0.45 μ m. The MB concentration was calculated using a UV-visible spectrometry (UV-1700 Pharma Spec, SHIMADZU, Kyoto, Japan). The relative MB concentration (C/C_0) was determined at the relative absorbance (A/A_0) of $\lambda = 662$ nm, according to the Beer-Lambert law, where A_0 and A were the absorbance of aqueous MB at a starting time (t_0) of photodegradation and at any time t , respectively.

The total organic carbon (TOC) was studied using Shimadzu TOC analyzer (TOC-VCPH, Kyoto, Japan). The oxidation and titration with potassium permanganate method was applied for the measurement of chemical oxygen demand (COD).

Table 1. Experimental conditions.

Methylene blue	30 mL, 5–20 mg/L
Photocatalyst	20 mg
Temperature	~30 °C
pH	Natural
Light source	Sunlight
Irradiation time	0–150 min

2.5. Detection of Active Species

To scrutinize the reactive species that was responsible for photocatalytic degradation of MB, three scavenger tests were done in the same procedure as discussed in the photodegradation experiment. In the scavenger tests, *di*-ammonium oxalate monohydrate, 2-propanol, and ascorbic acid were stipulated as h^+ , $\bullet OH$, and $\bullet O_2^-$ reactive species, respectively [29,30].

3. Results and Discussion

3.1. XRD Patterns Study

The crystal structure of the nanomaterials was confirmed by X-ray diffraction. Figure 1 displays the XRD patterns of the ZnO and with different copper contents CuO/ZnO nanocomposites. Major peaks were observed at around 31.82° (100), 34.50° (002), and 36.32° (101) of the undoped ZnO (JCPDS no.36-1451) [31]. CuO/ZnO nanocomposites displayed a very minor peak at 38.8°, which was indexed to the (111) of CuO [24]. With the addition of Cu in ZnO, the diffraction intensities and angles changed remarkably. The diffraction peak of CuO (111) was found with 5 and 7 wt % of copper content. In addition, with increased amounts of copper, no other peaks or appreciable shifts were observed and no solid solution was formed in between ZnO and CuO. The Scherrer equation was used to obtain the

grain size of the ZnO and CuO/ZnO nanocomposites. The estimated grains were found as ~32.16 and ~32.13 nm for ZnO and 5 wt % CuO/ZnO, respectively.

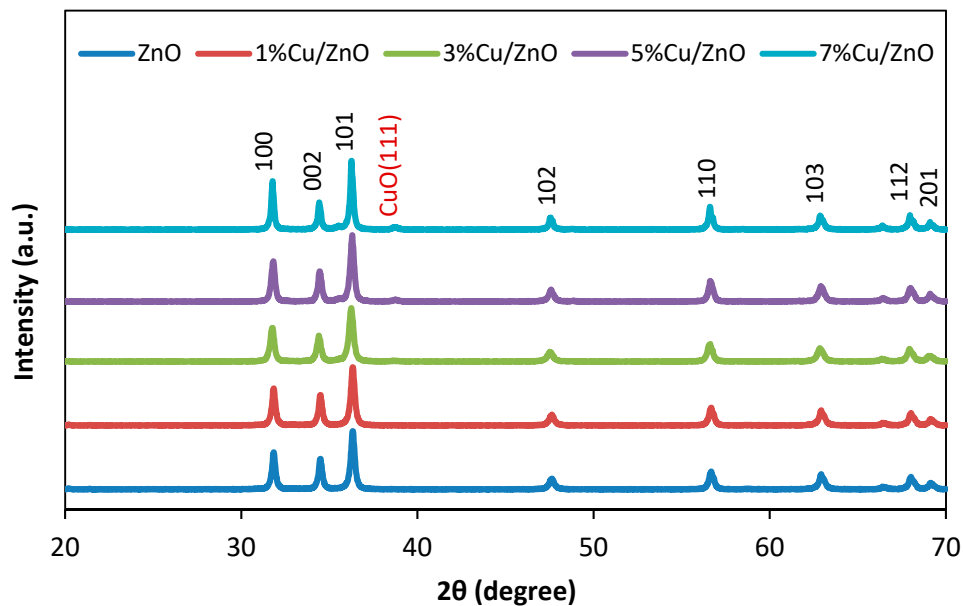


Figure 1. X-ray diffraction (XRD) patterns of ZnO and CuO/ZnO.

3.2. SEM and EDX Study

Crystal morphologies of the ZnO and CuO/ZnO were evaluated through SEM. Figure 2a shows that the synthesized ZnO was heterogeneous with rod-shaped branches of building blocks. On the other hand, Figure 2b shows that the shape of the CuO/ZnO composite changed from rod-like to spheroid. The particle sizes of synthesized composites were in the nanometer range, which was similar to the data of XRD. Figure 2c shows the EDX line-scanning values of CuO/ZnO heterojunction. The presences of copper, zinc, and oxygen atoms were exhibited by the EDX spectra analysis. Sharp peaks of Zn, Cu, and O were obtained; no other peak related to any other element was detected in the spectrum within the detection limit, which confirmed that synthesized materials were composed of Zn, Cu, and O only. The spectrum confirmed that Cu exists in the heterostructure, representing that the copper nanoparticles were successfully deposited on zinc oxide.

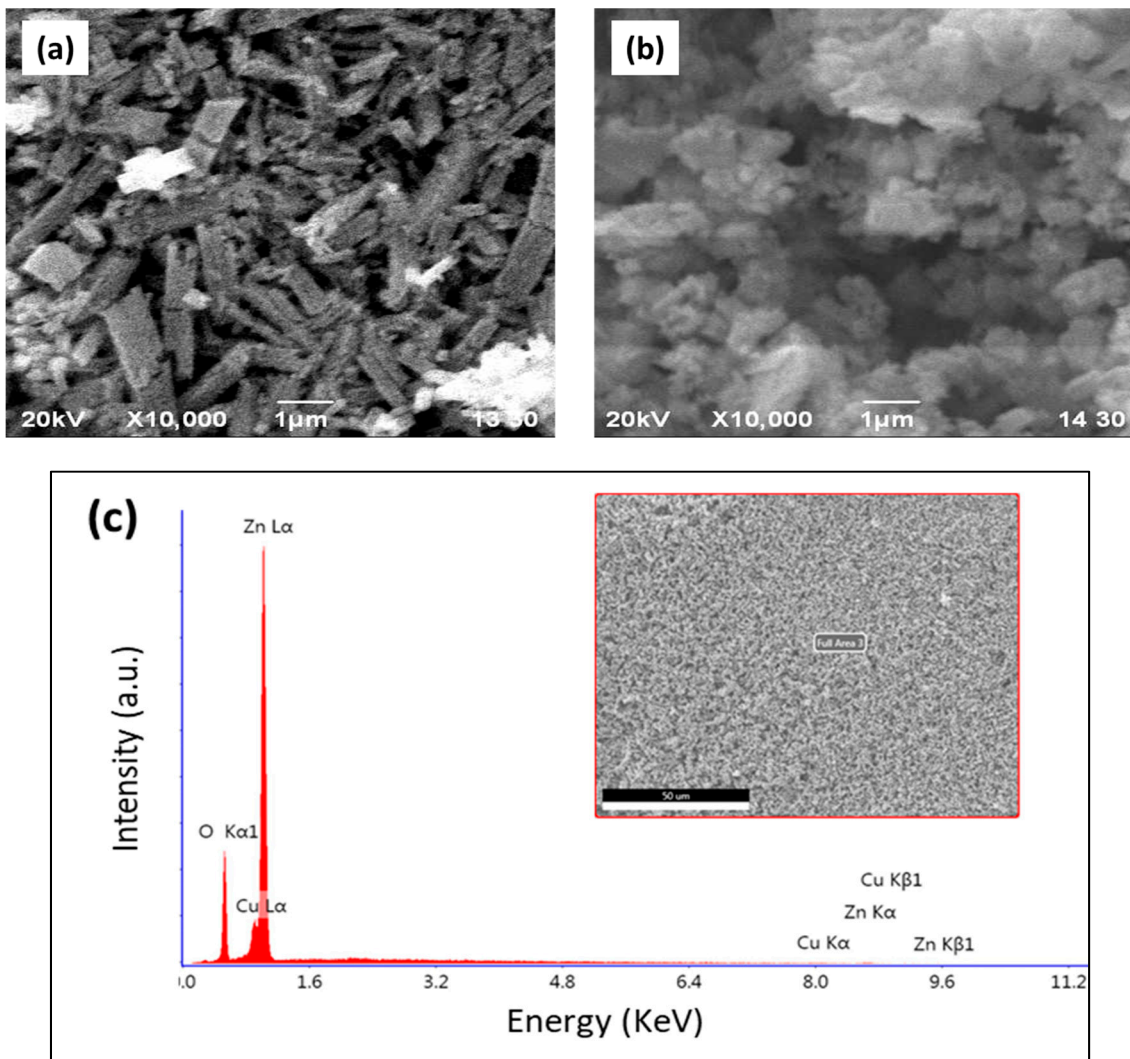


Figure 2. Scanning electron microscopy (SEM) images of (a) ZnO and (b) CuO/ZnO, and (c) energy-dispersive X-ray spectroscopy (EDX) pattern of CuO/ZnO.

3.3. FTIR Spectral Study

The FTIR spectra of ZnO and CuO/ZnO nanocomposites are depicted in Figure 3. Generally, the absorption bands of metal oxides were below 1000 cm^{-1} , due to inter-atomic vibrations. From Figure 3, it is seen that the absorption band of zinc oxide (stretching of Zn–O) was between 400 cm^{-1} and 590 cm^{-1} , which confirmed the wurtzite structure of ZnO [32]. The vibration around 3385 cm^{-1} and 1637 cm^{-1} was attributed to asymmetric and symmetric stretching H–O–H vibration, which was due to chemisorbed water. The very weak peak at 2320 cm^{-1} corresponded to the symmetric C–H bond vibrations, which may have been present due to the environmental conditions. Stretching modes of C–O appeared at 1110 cm^{-1} , because of the acetate group improper decomposition [33]. The bands of $3000\text{--}3650\text{ cm}^{-1}$ were attributed to reversible dissociative absorption of hydrogen on Zn and O [34].

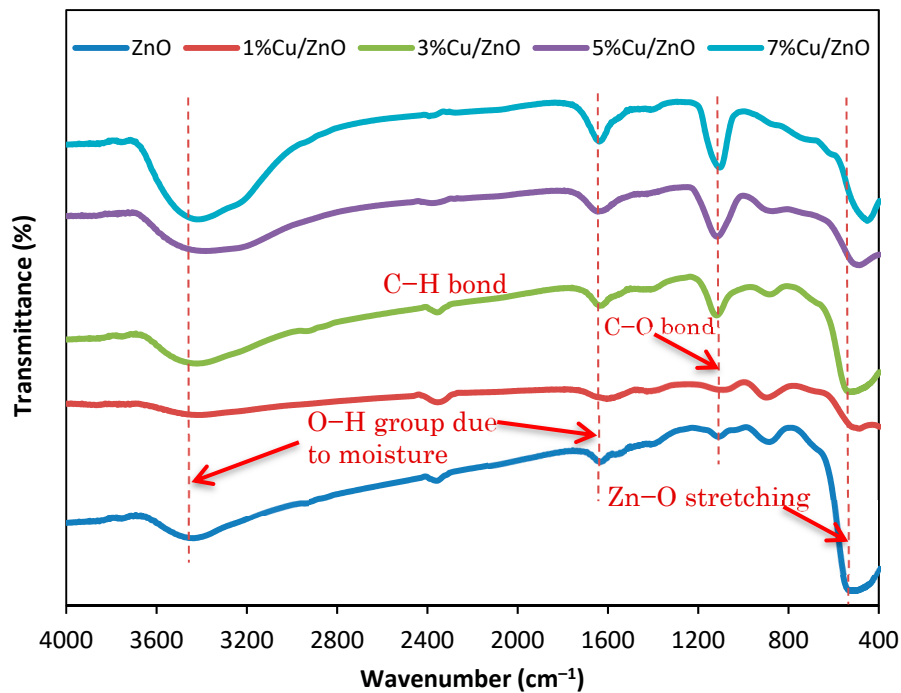


Figure 3. Fourier transform infrared (FTIR) spectra of ZnO and CuO/ZnO.

3.4. UV-VIS Spectral Changes

The absorption spectra of MB solution with CuO/ZnO under sunlight irradiation are shown in Figure 4. During photolysis, pure MB was exposed 150 min under sunlight and it was seen that the change of the absorption spectrum was negligible. The absorption spectrum at 662 nm slightly decreased under dark after 150 min with CuO/ZnO, indicating the MB dye adsorption on the composite. The well-defined absorption band disappeared after 150 min, which confirmed the MB degradation with CuO/ZnO in the presence of sunlight.

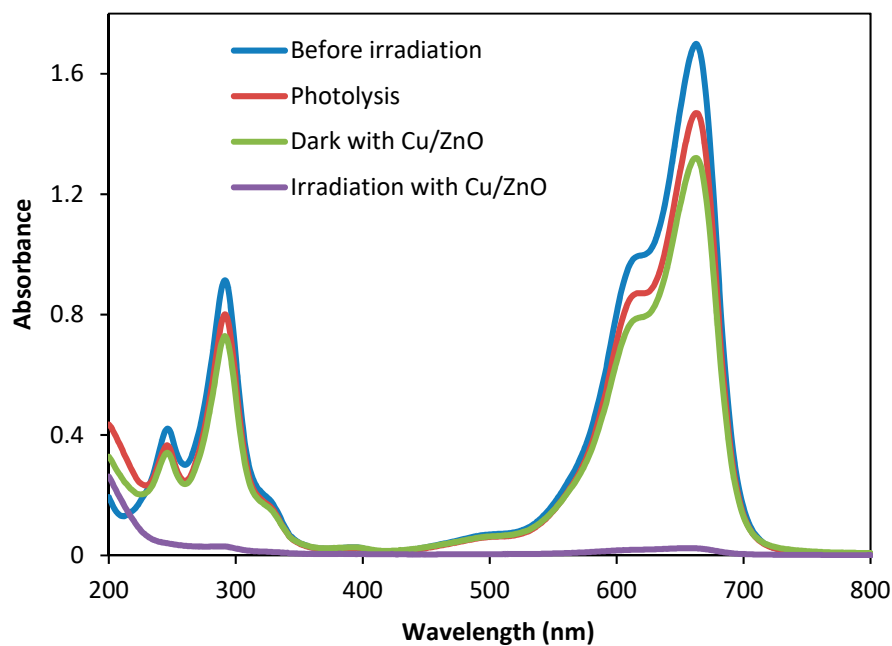


Figure 4. UV-visible spectral changes of methylene blue (MB) in water for before irradiation, photolysis, under dark, and sunlight irradiation.

3.5. Photocatalytic Dye Degradation

ZnO and CuO/ZnO were used in the presence of sunlight for the photodegradation of MB to evaluate the photocatalytic performance. The effect of the doping amounts of copper in the photodegradation of MB is depicted in Figure 5. The degradation rate increased with increasing copper amounts up to 5 wt % of the composite. More than 5 wt % of copper decreased the photocatalytic activity. This was because the ZnO surface was covered by the higher percentage of copper and reduced the sunlight absorption [35]. Due to efficient charge separation and higher electron transfer, 5 wt % CuO/ZnO composite showed better photocatalytic activity for MB degradation.

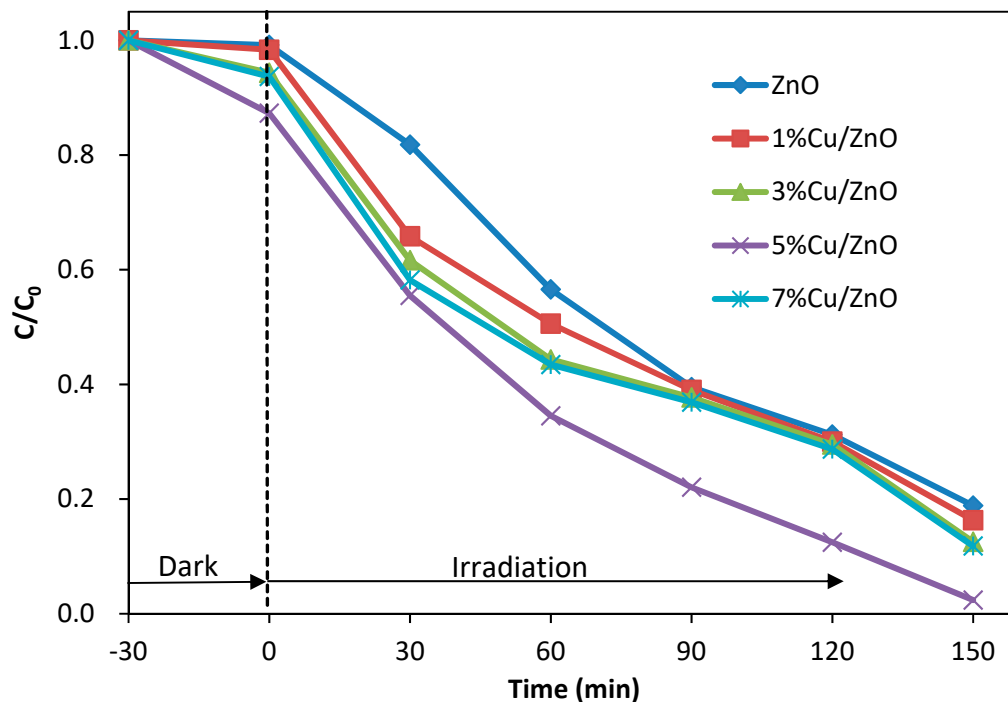


Figure 5. Photodegradation of MB by ZnO and CuO/ZnO using sunlight.

3.6. Effect of Initial Dye Concentration

The photocatalytic degradation of dye depended on its initial concentration, and it was necessary to investigate the effect of dye concentrations in view of their practical application. The solar photocatalytic degradation with different initial MB dye concentrations in the presence of CuO/ZnO was studied, as shown in Figure 6. It was observed that as initial MB dye concentrations increased from 5 mg/L to 20 mg/L, the dye degradation efficiency gradually decreased [36,37]. In this study, methylene blue of 10 mg/L solution was selected to evaluate the photodegradation of dye under sunlight, because of the high concentration of real wastewater.

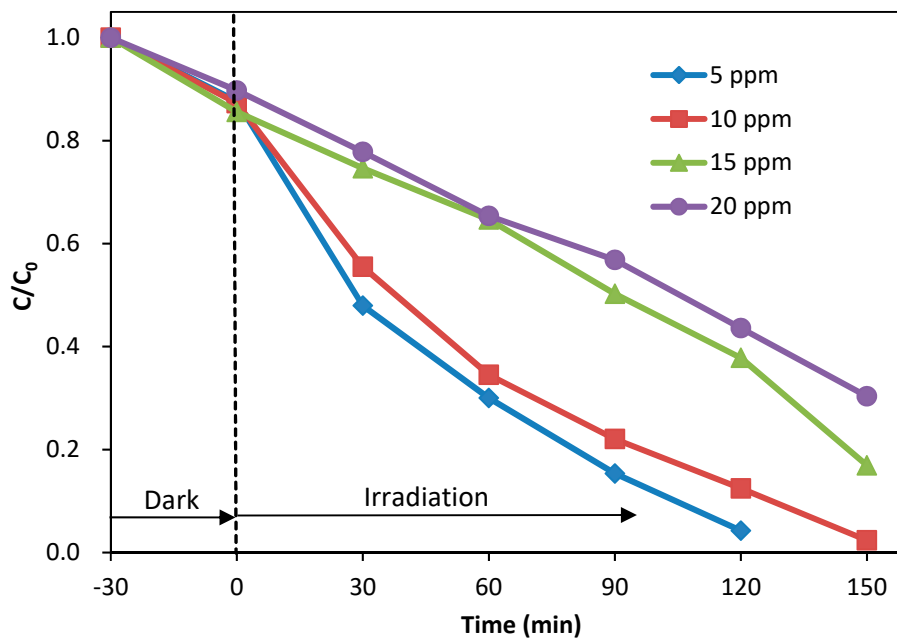


Figure 6. Effect of initial dye concentration on the photodegradation of MB with CuO/ZnO.

3.7. Role of Reactive Species

The scavengers of *di*-ammonium oxalate monohydrate (AO), 2-propanol, and ascorbic acid (AA) were used to identify the reactive species for MB photodegradation. The three scavengers' effect on the MB photodegradation with CuO/ZnO is displayed in Figure 7. From the results (Figure 7), it was observed that with the addition of 2-propanol, AO, and AA as a scavenger, photocatalytic degradation dropped from 66% (without scavenger) to 23% ($\bullet\text{O}_2^-$), 13% ($\bullet\text{OH}$), and 53% (h^+) for 1h, while the photocatalytic activity significantly decreased from 88% (without scavenger) to 29% ($\bullet\text{O}_2^-$), 37% ($\bullet\text{OH}$), and 79% (h^+) for 2 h irradiation, respectively. It can be surmised that the important roles played for the photodegradation of MB were by $\bullet\text{O}_2^-$ and $\bullet\text{OH}$ radicals, while a minor role was played by the h^+ radical in the degradation process under sunlight [38].

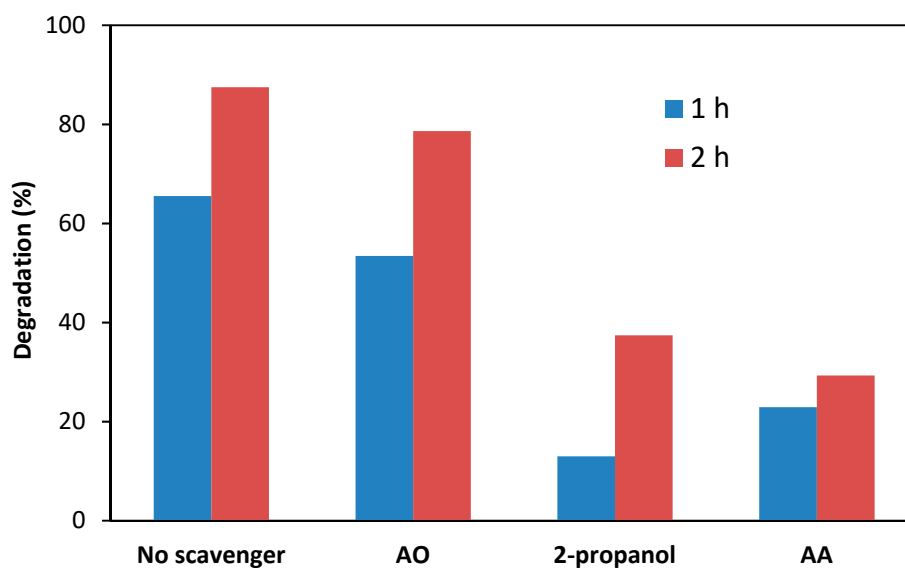


Figure 7. Effects of scavengers on the photodegradation of MB with CuO/ZnO using sunlight.

3.8. Degradation Mechanism

The schematic diagram (Figure 8) shows the photodegradation mechanism of MB with CuO/ZnO nanocomposite. CuO and ZnO formed a heterojunction, which assisted the separation of photogenerated carriers [39]. The conduction band (CB) potentials were -0.43 eV for CuO and -0.15 eV for ZnO vs Normal Hydrogen Electrode (NHE) [40]. The band gaps of CuO and ZnO were 1.4 and 3.23 eV, respectively [41,42]. During sunlight irradiation, CuO and ZnO were excited to generate electrons and holes at the CB and the valence band (VB), respectively, as displayed in Figure 8, since the band positions of ZnO were below the CB and VB of CuO. The photoexcited electrons transferred from CuO to ZnO, whereas the holes migrated from ZnO to CuO. [43]. Then, oxygen molecules in dye solution reacted with electrons to generate superoxide radical ($\cdot\text{O}_2^-$) and the holes combined with H_2O to produce hydroxyl radical ($\cdot\text{OH}$). Moreover, MB was directly oxidized by the holes at the VB of CuO [44,45]. The strong oxidant radicals of $\cdot\text{OH}$ and $\cdot\text{O}_2^-$ readily oxidized the MB molecule. We proposed the following possible degradation mechanism of MB with CuO/ZnO in the presence of sunlight.

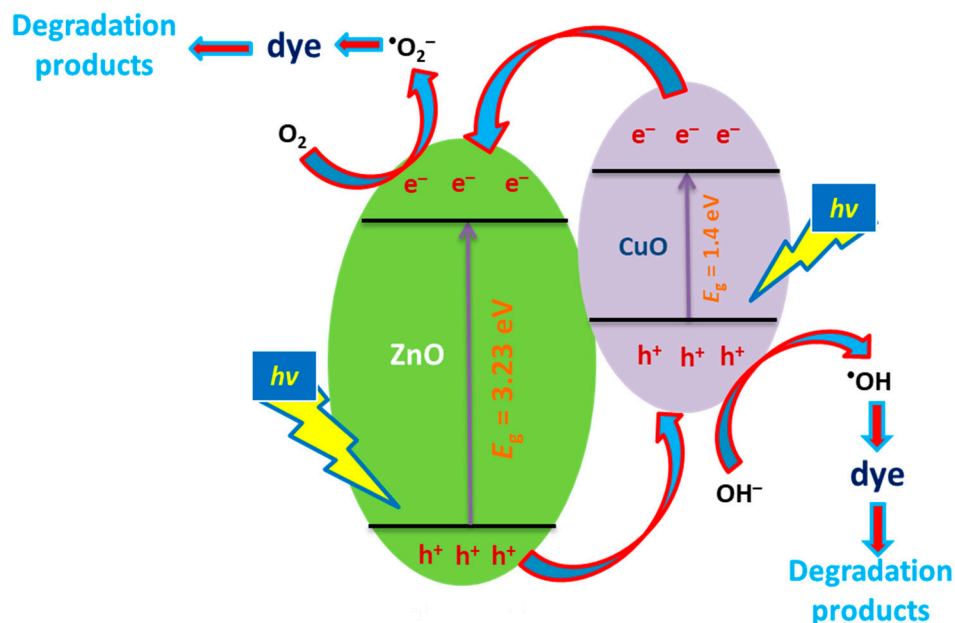
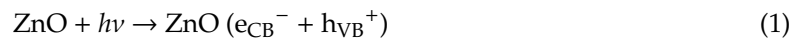


Figure 8. The possible degradation mechanism of CuO/ZnO photocatalyst using sunlight.

3.9. Mineralization of Dye

The evaluation of mineralization of MB was investigated by measuring the total organic carbon (TOC). The TOC removal is presented in Figure 9a, showing the degradation of MB under sunlight irradiation. The TOC rapidly decreased with increased solar irradiation time up to 2 h. After 7 h irradiation using CuO/ZnO, the mineralization of MB was observed at about 91% of TOC reduction. The chemical oxygen demand (COD) was an effective method, widely used for the measurement of

photodegradation of organic dye [46]. The test was used to measure the total amount of oxygen needed for the oxidation of dye to produce carbon dioxide and water [47]. The COD value of MB of aqueous solution using CuO/ZnO is described in Figure 9b. With increased solar irradiation time, COD values sharply decreased up to 3 h, and COD reduction was about 84% after 7 h. The reduction of COD and TOC values after the solar irradiation of MB indicated that methylene blue molecule was mineralized.

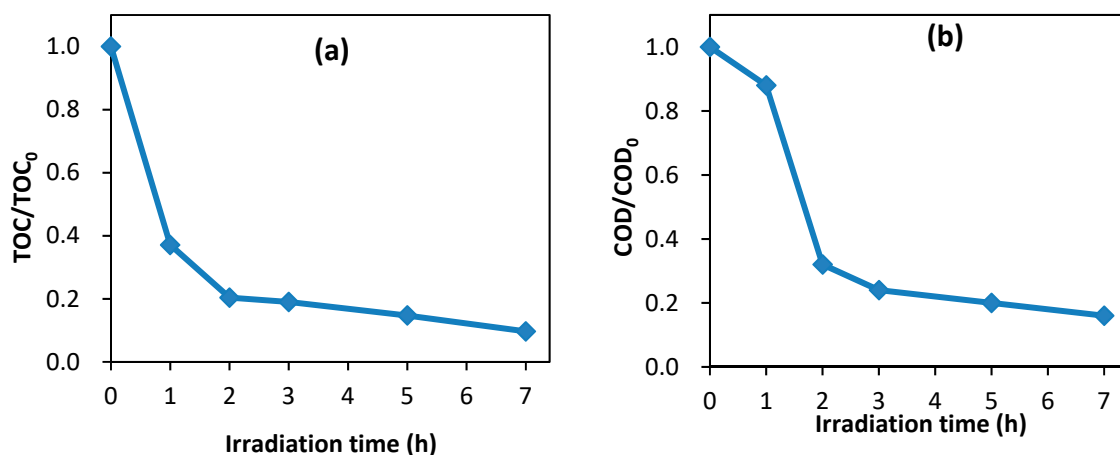


Figure 9. Mineralization of MB during the photodegradation with CuO/ZnO using sunlight. (a) total organic carbon (TOC) and (b) chemical oxygen demand (COD).

4. Conclusions

The low-cost mechanochemical combustion method was used to synthesize CuO/ZnO nanocomposites with various Cu contents. The best photodegradation efficiency was obtained with 5 wt % CuO/ZnO. The values of MB degrading with un-doped ZnO and CuO/ZnO were measured to be 81% and 98% respectively, after 2 h of solar irradiation. MB photodegradation with CuO/ZnO under sunlight occurred mainly with $\bullet\text{O}_2^-$ and $\bullet\text{OH}$ radicals, while the h^+ radical showed a minor role in the process. The decrease of TOC values of MB indicated the mineralization in the photocatalytic process. Therefore, sunlight photodegradation technology may be a more effective technique for textile wastewater treatment than photodegradation with artificial and expensive Hg-Xe lamp.

Author Contributions: M.A.I.M. conceived and designed the experiments and wrote the paper. A.A.M.S. performed the experiments. S.M.M., J.H., and R.I. analyzed the results.

Funding: This research was funded by the University Grants Commission of Bangladesh, grant number 6(76)UGC/S&T/Chemistry-02/2018/3577.

Acknowledgments: The authors are grateful to the Centre for Advanced Research in Sciences (CARS), University of Dhaka, Bangladesh for providing partial analytical support.

Conflicts of Interest: The authors declare no conflict of interest.

References

1. Mu, J.; Shao, C.; Guo, Z.; Zhang, Z.; Zhang, M.; Zhang, P.; Chen, B.; Liu, Y.C. High photocatalytic activity of ZnO-carbon nanofiber heteroarchitectures. *ACS Appl. Mater. Interfaces* **2011**, *3*, 590–596. [[CrossRef](#)] [[PubMed](#)]
2. Molla, M.A.I. Development of Advanced Technology for Photocatalytic Degradation of Organic Pollutants in Wastewater. Ph.D. Thesis, Mie University, Tsu, Japan, 2018.
3. Zangeneh, H.; Zinatizadeh, A.A.L.; Habibi, M.; Akia, M.; Isa, M.H. Photocatalytic oxidation of organic dyes and pollutants in wastewater using different modified titanium dioxides: A comparative review. *J. Ind. Eng. Chem.* **2015**, *26*, 1–36. [[CrossRef](#)]
4. Yulizar, Y.; Bakri, R.; Apriandanu, D.O.B.; Hidayat, T. ZnO/CuO nanocomposite prepared in one-pot green synthesis using seed bark extract of Theobroma cacao. *Nano Struct. Nano Objects* **2018**, *16*, 300–305. [[CrossRef](#)]

5. Vidic, J.; Stankic, S.; Haque, F.; Ciric, D.; Le Goffic, R.; Vidy, A.; Jupille, J.; Delmas, B. Selective antibacterial effects of mixed ZnMgO nanoparticles. *J. Nanopart. Res.* **2013**, *15*, 1595–1605. [[CrossRef](#)] [[PubMed](#)]
6. Lu, P.; Zhou, W.; Li, Y.; Wang, J.; Wu, P. Abnormal room temperature ferromagnetism in CuO/ZnO nanocomposites via hydrothermal method. *Appl. Surf. Sci.* **2017**, *399*, 396–402. [[CrossRef](#)]
7. Dorneanu, P.P.; Airinei, A.; Olaru, N.; Homocianu, M.; Nica, V.; Doroftei, F. Preparation and characterization of NiO, ZnO and NiO–ZnO composite nanofibers by electrospinning method. *Mater. Chem. Phys.* **2014**, *148*, 1029–1035. [[CrossRef](#)]
8. Hassanpour, M.; Hojaghan, H.S.; Niasari, M.S. Degradation of methylene blue and Rhodamine B as water pollutants via green synthesized Co₃O₄/ZnO nanocomposite. *J. Mol. Liq.* **2017**, *229*, 293–299. [[CrossRef](#)]
9. Hassanpour, M.; Salavati-Niasari, M.; Mousavi, S.A.; Safardoust-Hojaghan, H.; Hamadianian, M. CeO₂/ZnO Ceramic nanocomposites, synthesized via microwave method and used for decolorization of dye. *J. Nanostruct.* **2018**, *8*, 97–106.
10. Saravanan, R.; Karthikeyan, S.; Gupta, V.K.; Sekaran, G.; Narayanan, V.; Stephen, A. Enhanced photocatalytic activity of ZnO/CuO nanocomposite for the degradation of textile dye on visible light illumination. *Mater. Sci. Eng. C* **2013**, *33*, 91–98. [[CrossRef](#)]
11. Saravanan, R.; Gupta, V.K.; Mosquera, E.; Gracia, F. Preparation and characterization of V₂O₅/ZnO nanocomposite system for photocatalytic application. *J. Mol. Liq.* **2014**, *198*, 409–412. [[CrossRef](#)]
12. Saravanan, R.; Gupta, V.K.; Narayanan, V.; Stephen, A. Visible light degradation of textile effluent using novel catalyst ZnO/γ-Mn₂O₃. *J. Taiwan Inst. Chem. Eng.* **2014**, *45*, 1910–1917. [[CrossRef](#)]
13. Li, B.; Wang, Y. Facile synthesis and photocatalytic activity of ZnO–CuO nanocomposite. *Superlattice Microst.* **2010**, *47*, 615–623. [[CrossRef](#)]
14. Kuriakose, S.; Avasthi, D.K.; Mohapatra, S. Effects of swift heavy ion irradiation on structural, optical and photocatalytic properties of ZnO–CuO nanocomposites prepared by carbothermal evaporation method. *Beilstein J. Nanotechnol.* **2015**, *6*, 928–937. [[CrossRef](#)]
15. Wang, A.; Chen, Z.; Zheng, Z.; Xu, H.; Wang, H.; Hu, K.; Yan, K. Remarkably enhanced sulfate radical-based photo-Fenton-like degradation of levofloxacin using the reduced mesoporous MnO@MnOx microspheres. *Chem. Eng. J.* **2019**, *379*, 122340. [[CrossRef](#)]
16. Gnanasekaran, L.; Hemamalini, R.; Saravanan, R.; Qin, J.; Yola, M.L.; Atar, N.; Gracia, F. Nanosized Fe₃O₄ incorporated on a TiO₂ surface for the enhanced photocatalytic degradation of organic pollutants. *J. Mol. Liq.* **2019**, *287*, 110967. [[CrossRef](#)]
17. Saravanan, R.; Agarwal, S.; Gupta, V.K.; Khan, M.M.; Gracia, F.; Mosquera, E.; Narayanan, V.; Stephen, A. Line defect Ce³⁺ induced Ag/CeO₂/ZnO nanostructure for visible-light photocatalytic activity. *J. Photochem. Photobiol. A Chem.* **2018**, *353*, 499–506. [[CrossRef](#)]
18. Jebaranjitham, J.N.; Mageshwari, C.; Saravanan, R.; Mu, N. Fabrication of amine functionalized graphene oxide–AgNPs nanocomposite with improved dispersibility for reduction of 4-nitrophenol. *Compos. Part B* **2019**, *171*, 302–309. [[CrossRef](#)]
19. Qin, J.; Yang, C.; Cao, M.; Zhang, X.; Saravanan, R.; Limpanart, S.; Ma, M.; Liu, R. Two dimensional porous sheet-like carbon-doped ZnO/g-C₃N₄ nanocomposite with high visible-light photocatalytic performance. *Mater. Lett.* **2017**, *189*, 156–159. [[CrossRef](#)]
20. Saravanan, R.; Khan, M.M.; Gracia, F.; Qin, J.; Gupta, V.K.; Arumainathan, S. Ce³⁺-ion-induced visible-light photocatalytic degradation and electrochemical activity of ZnO/CeO₂ nanocomposite. *Sci. Rep.* **2016**, *6*, 31641. [[CrossRef](#)]
21. Yang, C.; Xue, Z.; Qin, J.; Sawangphruk, M.; Saravanan, R.; Zhang, X.; Liu, R. Visible-light Driven Photocatalytic H₂ Generation and Mechanism Insights on Bi₂O₂CO₃/G-C₃N₄ Z-scheme Photocatalyst. *Phys. Chem. C* **2019**, *123*, 4795–4804. [[CrossRef](#)]
22. Kanade, K.G.; Kale, B.B.; Baeg, J.O.; Lee, S.M.; Lee, C.W.; Moon, S.J.; Chang, H. Self-assembled aligned Cu doped ZnO nanoparticles for photocatalytic hydrogen production under visible light irradiation. *Mater. Chem. Phys.* **2007**, *102*, 98–104. [[CrossRef](#)]
23. Rooydell, R.; Brahma, S.; Wang, R.C.; Modaberi, M.R.; Ebrahimzadeh, F.; Liu, C.P. Cu doped ZnO nanorods with controllable Cu content by using single metal organic precursors and their photocatalytic and luminescence properties. *J. Alloys Compd.* **2017**, *691*, 936–945. [[CrossRef](#)]
24. Hsieh, S.-H.; Ting, J.-M. Characterization and photocatalytic performance of ternary Cu-doped ZnO/Graphene materials. *Appl. Surf. Sci.* **2018**, *427*, 465–475. [[CrossRef](#)]

25. Phiwdang, K.; Suphankij, S.; Mekprasart, W.; Pecharapa, W. Synthesis of CuO nanoparticles by precipitation method using different precursors. *Energy Procedia* **2013**, *34*, 740–745. [[CrossRef](#)]
26. Jun, S.T.; Choi, G.M. Composition dependence of the electrical conductivity of ZnO(n)–CuO(p) ceramic composite. *J. Am. Ceram. Soc.* **1998**, *81*, 695–699. [[CrossRef](#)]
27. Zhang, D. Synthesis and characterization of ZnO-doped cupric oxides and evaluation of their photocatalytic performance under visible light. *Transit. Met. Chem.* **2010**, *35*, 689–694. [[CrossRef](#)]
28. Molla, M.A.I.; Furukawa, M.; Tateishi, I.; Katsumata, H.; Kaneco, S. Studies of effects of calcination temperature on the crystallinity and optical properties of Ag-doped ZnO nanocomposites. *J. Compos. Sci.* **2019**, *3*, 18. [[CrossRef](#)]
29. Benavente, E.; Duran, F.; Sotomayor-Torres, C.; Gonzalez, G. Heterostructured layered hybrid ZnO/MoS₂ nanosheets with enhanced visible light photocatalytic activity. *J. Phys. Chem. Solids* **2018**, *113*, 119–124. [[CrossRef](#)]
30. Su, J.; Zhu, L.; Geng, P.; Chen, G. Self-assembly graphitic carbon nitride quantum dots anchored on TiO₂ nanotube arrays: An efficient heterojunction for pollutants degradation under solar light. *J. Hazard. Mater.* **2016**, *316*, 159–168. [[CrossRef](#)] [[PubMed](#)]
31. Lamba, R.; Umar, A.; Mehta, S.K.; Kansal, S.K. Sb₂O₃–ZnO nanospindles: A potential material for photocatalytic and sensing applications. *Ceram. Int.* **2015**, *41*, 5429–5438. [[CrossRef](#)]
32. Khana, S.A.; Noreen, F.; Kanwal, S.; Iqbal, A.; Hussain, G. Green synthesis of ZnO and Cu-doped ZnO nanoparticles from leaf extracts of *Abutilon indicum*, *Clerodendrum infortunatum*, *Clerodendrum inerme* and investigation of their biological and photocatalytic activities. *Mater. Sci. Eng. C* **2018**, *82*, 46–59. [[CrossRef](#)] [[PubMed](#)]
33. Saravanakkumar, D.; Sivaranjani, S.; Kaviyarasu, K.; Ayeshamariam, A.; Ravikumar, B.; Pandiarajan, S.; Veeralakshmi, C.; Jayachandran, M.; Maaza, M. Synthesis and characterization of ZnO–CuO nanocomposites powder by modified perfume spray pyrolysis method and its antimicrobial investigation. *J. Semicond.* **2018**, *39*, 033001. [[CrossRef](#)]
34. Ma, G.; Liang, X.; Li, L.; Qiao, R.; Jiang, D.; Ding, Y.; Chen, H. Cu-doped zinc oxide and its polythiophene composites: Preparation and antibacterial properties. *Chemosphere* **2014**, *100*, 146–151. [[CrossRef](#)] [[PubMed](#)]
35. Molla, M.A.I.; Furukawa, M.; Tateishi, I.; Katsumata, H.; Kaneco, S. Fabrication of Ag-doped ZnO by mechanochemical combustion method and their application into photocatalytic Famotidine degradation. *J. Environ. Sci. Health Part A* **2019**, *54*, 914–923. [[CrossRef](#)] [[PubMed](#)]
36. Kaneco, S.; Li, N.; Itoh, K.-K.; Katsumata, H.; Suzuki, T.; Ohta, K. Titanium dioxide mediated solar photocatalytic degradation of thiram in aqueous solution: Kinetics and mineralization. *Chem. Eng. J.* **2009**, *148*, 50–56. [[CrossRef](#)]
37. Molla, M.A.I.; Ahsan, S.; Tateishi, I.; Furukawa, M.; Katsumata, H.; Suzuki, T.; Kaneco, S. Degradation, Kinetics, and Mineralization in the solar photocatalytic treatment of aqueous amitrole solution with titanium dioxide. *Environ. Eng. Sci.* **2018**, *35*, 401–407. [[CrossRef](#)]
38. Wang, A.; Wang, H.; Deng, H.; Wang, S.; Shi, W.; Yi, Z.; Qiu, R.; Yan, K. Controllable synthesis of mesoporous manganese oxide microsphere efficient for photo-Fenton-like removal of fluoroquinolone antibiotics. *Appl. Catal. B Environ.* **2019**, *248*, 298–308. [[CrossRef](#)]
39. Chabri, S.; Dhara, A.; Show, B.; Adak, D.; Sinha, A.; Mukherjee, N. Mesoporous CuO-ZnO p-n heterojunction based nanocomposites with high specific surface area for enhanced photocatalysis and electrochemical sensing. *Catal. Sci. Technol.* **2016**, *6*, 3238–3252. [[CrossRef](#)]
40. Yang, L.; Xie, C.S.; Zhang, G.Z.; Zhao, J.W.; Yu, X.L.; Zeng, D.W.; Zhang, S.P. Enhanced response to NO₂ with CuO/ZnO laminated heterostructured configuration. *Sens. Actuator B* **2014**, *195*, 500–508. [[CrossRef](#)]
41. Alsabahi, J.; Bora, T.; Alabri, M.; Dutta, J. Efficient visible light photocatalysis of benzene, toluene, ethylbenzene and xylene (BTEX) in aqueous solutions using supported zinc oxide nanorods. *PLoS ONE* **2017**, *12*, e0189276.
42. Hansen, B.J.; Kouklin, N.; Lu, G.H.; Lin, I.; Chen, J.H.; Zhang, X. Transport, analyte detection, and opto-electronic response of p-Type CuO nanowires. *J. Phys. Chem. C* **2010**, *114*, 2440–2447. [[CrossRef](#)]
43. Zhang, J.N.; Chen, T.H.; Yu, J.H.; Liu, C.; Yang, Z.B.; Lu, H.B.; Yin, F.; Gao, J.Z.; Liu, Q.R.; Zhang, X.W.; et al. Enhanced photocatalytic activity of flowerlike CuO-ZnO nanocomposites synthesized by one-step hydrothermal method. *J. Mater. Sci.* **2016**, *27*, 10667–10672. [[CrossRef](#)]

44. Harish, S.; Archana, J.; Sabarinathan, M.; Navaneethan, M.; Nisha, K.D.; Ponnusamy, S.; Muthamizhchelvan, C.; Ikeda, H.; Aswal, D.K.; Hayakawa, Y. Controlled structural and compositional characteristic of visible light active ZnO/CuO photocatalyst for the degradation of organic pollutant. *Appl. Surf. Sci.* **2017**, *418*, 103–112. [[CrossRef](#)]
45. Wu, F.S.; Wang, X.H.; Hu, S.Z.; Hao, C.; Gao, H.W.; Zhou, S.S. Solid-state preparation of CuO/ZnO nanocomposites for functional supercapacitor electrodes and photocatalysts with enhanced photocatalytic properties. *Int. J. Hydrogen Energy* **2017**, *42*, 30098–30108. [[CrossRef](#)]
46. Li, J.; Chen, C.; Zhao, J.; Zhu, H.; Orthman, J. Photodegradation of dye pollutants on TiO₂ nanoparticles dispersed in silicate; UV-Vis irradiation. *Appl. Catal. B Environ.* **2002**, *37*, 331–338. [[CrossRef](#)]
47. Jain, R.; Shirkarwar, S. Removal of hazardous dye Congo-red removal from waste material. *J. Hazard. Mater.* **2008**, *152*, 942–948. [[CrossRef](#)]



© 2019 by the authors. Licensee MDPI, Basel, Switzerland. This article is an open access article distributed under the terms and conditions of the Creative Commons Attribution (CC BY) license (<http://creativecommons.org/licenses/by/4.0/>).